**Signal Processing and Renewable Energy**
September 2023, (pp. 95-112)
ISSN: 2588-7327
eISSN: 2588-7335

# Robust H Infinity Control of Micro-Grid to Develop the Power Management Performance

**Amin Mavali [1], Ali Naderi Saatlo [1*]**

[1] Department of Electrical-Electronics Engineering Urmia Branch, Islamic Azad University, Urmia, Iran.

Received: 29-May-2023, Revised: 01-Agu-2023, Accepted: 27-Agu-2023.

**Abstract**

In this paper, to develop the dynamic performance of an islanding mode micro-grid, which contains a wind turbine unit and a gas distributed generation (DG), simultaneous usage of H infinity and robust control are presented. By using the doubly-fed induction generator (DFIG) and the variable speed wind turbine, the system inertia is decreased and then the dynamic stability is also decreased. The virtual inertia implementation in DFIG causes the power system stability improvement. However, the major challenge that should be considered is the change in the system parameters or uncertainties, when the virtual inertia is employed. In this paper, the implementation of virtual inertia in the DFIG control system is described in detail and the impact of uncertainties and changes in the control system parameters over the performance of the frequency control system are investigated. In order to improve the dynamic stability and the steady state performance of the frequency control system, benefiting from the impact of virtual inertia, the mixed robust H infinity control approach is proposed. The simulation results using MATLAB software show that the proposed hybrid controller guarantees system stability in conditions of uncertainties and with the variation of the control system parameters.

**Keywords:** H Infinity, Power Management, DG, Robust, Micro-Grid, Control.

## 1. INTRODUCTION

Nowadays, renewable energy resources play a major role in electrical energy supplement. Wind energy could be mentioned as one of the most important of these useful energies. Considering variations in wind speed and consequently this effect on output power in wind turbines, there are some methods to extract the maximum power such as DFIG [1]. It cannot used to utilize wind turbo generators for frequency control in micro-grids, because of wind speed variation and its sudden substance. These kinds of outspread

***Corresponding Authors Email: a.naderi@iaurmia.ac.ir

energy production in the viewpoint of power and frequency control are called non-dispatchable. Indeed, to achieve frequency control in micro-grids, especially in islanding mode, outspread energy resources are used such as gas or diesel turbo generators. At these turbo generators, governor speed operates as the responsible of frequency control [2]. The individual adjustable factor in common Load Frequency Control (LFC) systems is droop coefficients that are related to governor speed. Low values of droop coefficients cause deviance frequency reduction rather than nominal value in Steady State (SS) and improve the steady response of the load-frequency control system. By the way, droop coefficients with low values cause variation in frequency increment in transient mode and it could unstable the system in case of either islanding mode or load variation [3].

Since synchronous generators which are connected to the grid have much great inertia, low time frequency variations lead to dynamic grid stability increment. Synchronous generators in general respond to the frequency variations system so as grid frequency decreases output generator power increases by the case of kinetic energy releasing for a short time. This short-time power increases compensations gird requirement and prevents high sudden frequency loss. But at DFIGs, there are some power electronic instruments and wind turbine rotation speed is not related to grid frequency, thus grid frequency variations are not seen by the rotor. Therefore, by using variable speed generators connected to wind turbines, other uncontrollable outspread generation resources and nominal inertia decreases because of less consumption of synchronous generators.

There has been wide research to improve micro-grid dynamic stability in islanding mode and also global connection conditions [4]. To reduce short-time frequency variations and micro-grid dynamic stability improvement, using batteries or energy storages are being suggested. In this way, controllable outspread generation resources, adjust and control micro-grid frequency in steady state, and batteries reduce short-time frequency variations. Although storage equipment improves load-frequency system dynamic operation, their inverters cause expanse increment [5-7].

Operating virtual inertia in DFIG dynamic behavior of micro-grids has been improved. In [8-11] a high-level capacitor is used as a virtual inertia resource. This method also is expensive due to additional equipment. In [10] and [11], the section rotating mass inertia of the wind turbo generator is used to operate virtual inertia. Although virtual inertia operation using rotating mass does not need additional equipment and expanse, using this method has some limitations. In this mode, virtual inertia values depend on the rotor speed of DFIG at the frequency shift moment. Since rotor speed depends on wind speed and is unpredictable, the impact of this method is different at short-time frequency variation reduction. At low and high wind speeds, this method could not be used due to wind turbine stopping situations. Another limitation of virtual inertia operation using rotating mass is thermal limitation. If there are variations in system frequency at high wind speeds, the generator will produce additional power by

virtual inertia control loop operation, generator temperature will increase that may be over-ranged.

The main point that should be considered in load-frequency control system operation evaluation with virtual inertia, is system factors uncertainties. Some factors could be mentioned such as governor droop factor uncertainties, wind speed variations, unpredictability, and inertia variations. If different factors and uncertainties in the system model are ignored, it may cause delusive results as marginal targets will not occur well and static and dynamic system behavior will not be expected [12].

Although uncertainty factors' impact on common load-frequency control systems has been evaluated in many papers and some control strategies are suggested to improve system operation with uncertainties like optimized control [13], sliding mode control [14], and intelligent control [15-16], a considering piece of research has not implemented yet when virtual inertia participates in load-frequency control. In [17], considering some disturbances and system parameters uncertainty, some insulate controllers like $H_\infty$ and $\mu$ synthesis are used for secondary frequency control loop improvement. In [18], the system disturbances are considered as an uncertainty, then strict controller $H_\infty$ is suggested for a load-frequency control loop in a bisection system. One of the other methods suggested for frequency system stability improvement is a virtual impedance loop [19] and frequency control is allowed for linear system equations and energy storage at the same time [20].

In this paper, virtual inertia and strict control in micro-grids usage are proposed. Virtual inertia will be added to a DFIG control system in this paper and robust control will be added to a gas turbo generator. In section (2), the virtual inertia accomplishment method in DFIG is explained. In section (3), while introducing the understudy micro-grid, it will be indicated that gas turbo generator governor droop coefficients uncertainty and virtual inertia value that are resulted by wind generator mass rotating equipped with DFIG, influence the load-frequency control system and may lead to the system instability. In order to improve the load-frequency control system, especially in terms of dynamic micro-grid stability, besides the virtual inertia usage, a robust $H_\infty$ approach is used in the frequency control system in this paper. The specifications of the designed controller will be explained in section (4). Simulation results in section (5) indicate that virtual inertia and strict $Robust\ H_\infty$ controller usage improve the micro–grid dynamic stability and supports system stability when there are control factors uncertainty.

## 2. VIRTUAL INERTIA ACCOMPLISHMENT IN DFIG

In DFIGs, the stator is connected to the grid directly, and the rotor is connected via two back-to-back converters. The rotor side converter is controlled so that besides stator voltage adjustment, maximum power is obtained at different wind speeds. The grid side converter adjusts capacitor voltage between two converters. Just like synchronous generators, wind turbines also have much kinetic energy in rotating mass. However, wind turbines with variable speed

cannot release their inertia and impose the resulting energy to the grid due to the grid frequency detachment from turbine speed, and turbine speed control to track maximum power point tracking in different wind speeds.

Wind turbine Maximum Power Point Tracking (MPPT) $P_m^{opt}$ can be shown as a three-degree function of wind turbine shaft mechanical speed as follows:

$$J = \left(\sigma + \varepsilon_0 \varepsilon_r \frac{\partial}{\partial t}\right) E + J_e \qquad (1)$$

In this equation, $K_{opt}$ is a factor that depends on the wind turbine wing angle. Thus, if the turbine wing angle is constant, we can suppose $K_{opt}$ as a constant value. The rotor side converter is controlled so that output electrical power tracking $P_m^{opt}$value can be controlled as well. If the rotor side converter controller reacts too fast, we can suppose output electrical power is the same as maximum power point tracking.

On the other hand, in a turbo generator input mechanical power $P_m$is related to output mechanical power $P_e$via the following equation:

$$P_m - P_e = \frac{d}{dt}\left(\frac{1}{2} J\omega_m^2\right) = J\omega_m \frac{d\omega_m}{dt} \qquad (2)$$

In this equation, $J$ is the inertia value of the rotating mass connected to the turbo generator shaft. In synchronous generators, input mechanical power is controlled by the governor to achieve frequency control. It results that the mechanical turbo generator speed shaft $\omega_m$that determines the system frequency, participates in output electrical power directly. In DFIGs, unlike synchronous generators, output electrical power is controlled directly. So, differences in system frequency and rotating mass inertia do not affect on output electrical power. Equation 2 can be shown as per unit:

$$P_m - P_e = 2H\omega_m \frac{d\omega_m}{dt} \qquad (3)$$

As shown, $H$ is wind turbo generator inertia constant and its unit is second and $P_e$ is the same as $P_m^{opt}$. $P_m$ value is uncontrollable and depends on wind speed. Thus, in equation (3) $\omega_m$ is a variable value that depends on wind speed and does not depend on system frequency.

An accurate and intact model of a wind turbo generator equipped with DFIG contains 15 particular values, in a way that one of them is much less than the others. Then we can estimate wind turbo generator as a first-order system. Sensitivity analysis and participation factor show that $\omega_m$ and $H$ value have a huge effect on the dominant pole.

Equation 3 linearization around operation point $\omega_{m0}$ results in the following relation:

$$\Delta P_m - \Delta P_e = 2H\omega_m \frac{d\Delta\omega_m}{dt} \qquad (4)$$

In equation (4), $\Delta P_e$ determines as follows:

$$\Delta P_e = 3K_{opt}\omega_{m0}^2 \Delta\omega_m \qquad (5)$$

For virtual inertia accomplishment, output electrical power control is different, so that in addition to MPPT, it responds to system frequency changes. Therefore equation 5 is corrected as follows:

$$\Delta P_e = 3K_{opt}\omega_{m0}^2\Delta\omega_m - H_v(s)\omega_{m0}\Delta\omega \quad (6)$$

In equation (6), $\omega$ is the angle frequency system and $H_v(s)$ is a virtual inertia transfer function. Since the inertia function operates as a differential on system frequency, the function $H_v(s)$ is written as follows:

$$H_v(s) = \frac{M_v}{(1+s\tau_1)(1+s\tau_2)} \quad (7)$$

At the transfer function $M_v$ is virtual inertia constant, $\tau_1$ and $\tau_2$ are virtual inertia timing constants. The main reason for this transfer function usage for virtual inertia accomplishment is the operation on low frequencies as a differential. If equation (6) is replaced in equation (4), then we have:

$$\Delta P_e = 3K_{opt}\omega_{m0}^2\Delta\omega_m - H_v(s)\omega_{m0}\Delta\omega + 2H\omega_0\Delta\omega_m \quad (8)$$

Using above equation $\Delta\omega_m$ is obtained as follows:

$$\Delta\omega_m = \frac{1}{2H\omega_0 s + 3K_{opt}\omega_{m0}^2}\Delta P_m + \frac{H_v(s)\omega_{m0}}{2H\omega_0 s + 3K_{opt}\omega_{m0}^2}\Delta\omega \quad (9)$$

Substituting equation (9) into equation (6):

$$\Delta P_e = \frac{3K_{opt}\omega_{m0}^2}{2H\omega_0 + 3K_{opt}\omega_{m0}^2}\Delta P_m - \frac{2HH_v(s)\omega_{m0}s}{2Hs + 3K_{opt}\omega_{m0}}\Delta\omega \quad (10)$$

As shown in equations (9) and (10), virtual inertia just causes mechanical speed and output electrical power shift when there is a system frequency shift and mechanical speed would not be zero at the same time. If we determine $\omega_{m0}$ as zero, $M_v$ value would be zero too and wind turbo generators would work without virtual inertia. Using the virtual inertia in DFIGs control system, output electrical generator power on low frequencies is shown as follows:

$$P_e = P_m^{opt} - M_v\omega_{m0}\frac{d\omega}{dt} \quad (11)$$

## 3. UNDERSTUDY MICRO-GRID

The understudy micro-grid in this paper is shown in figure 1 that consists of two outspread generation unit. Unit 1 is a wind turbine equipped with DFIG with 2.5 MVA capacity and unit 2 is a gas turbo generator with 2.5 MVA capacity equipped with frequency control system. Load and lines specifications is denoted in reference 3. As it is shown in figure 2 when we disconnect switch b2 the micro-grid detaches from principle grid and operates on islanding mode. $G_1(s)$ and $G_1(s)$ transfer function in order equals the first and second part of equation 10. Factors value used in block diagram, is denoted in table 1.

In the understudy system, the gas turbo generator controls the frequency. Since power produced by the wind turbine is variant due to wind speed variation, the system frequency shift is evitable. By the way. the appropriate function of the frequency control system that is droop control, has a major importance in wind turbines with variant speed.

Equation 12 realized as a droop equation indicates frequency shift relation with power shift on steady mode:

**Table 1.** ***Used factors value in understudy system for transfer functions [17].***

| Parameter | $T_G(s)$ | $T_T(s)$ | $T_S(s)$ | $H$ | $K_{opt}$ | $K_S$ |
|---|---|---|---|---|---|---|
| Value | 0.81 | 0.49 | 2.9 | 2.8 | 0.742 | 1.7 |

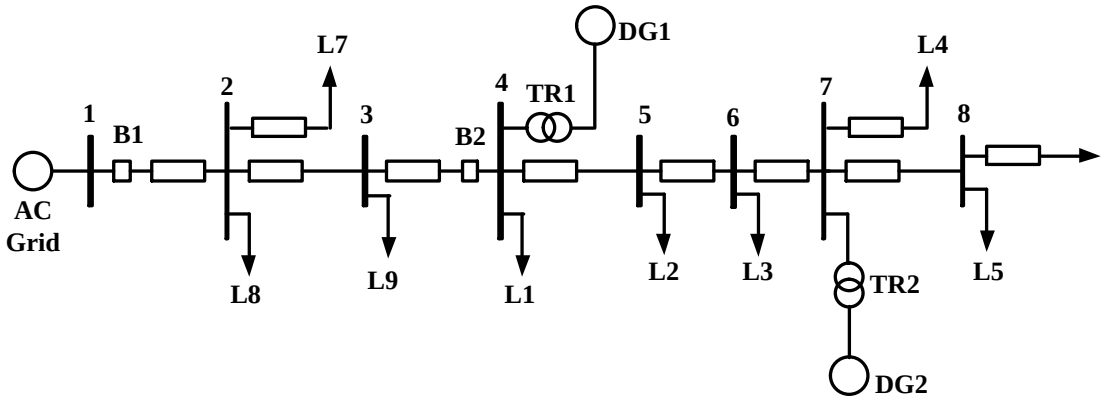


***Fig. 1. Microgrid under consideration [17].***

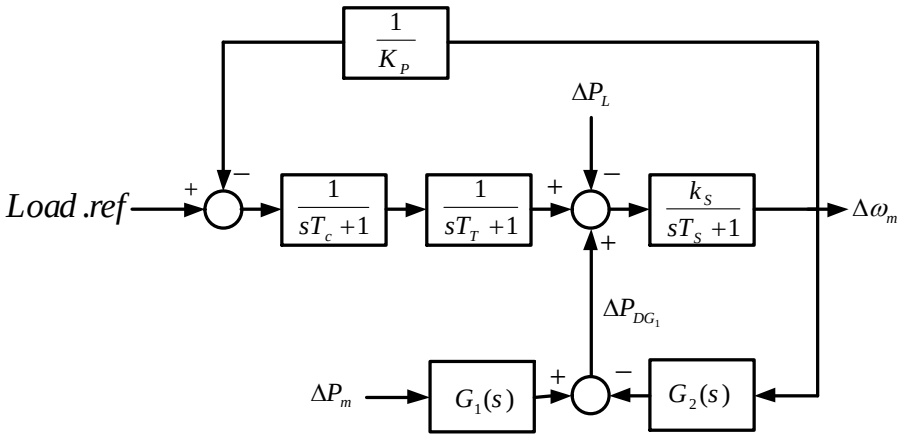


***Fig. 2. Understudy micro-grid block diagram.***

$$\omega - \omega_0 = -K_p(P - P_0) \qquad (12)$$

As noticed above the less $K_p$ value the better frequency adjustment on steady mode. Although as $K_p$ shrinks dynamic system stability castrates. Figure 3 indicates the root locus due to $K_p$ factor value shift without any virtual inertia. At understudy micro-grid instability boundary via $K_p$ value is 107 and fewer values cause micro-grid instability. Figure 4 shows the virtual inertia addition effect on the root locus. In this mode $M_v$ is equaled 50 seconds.

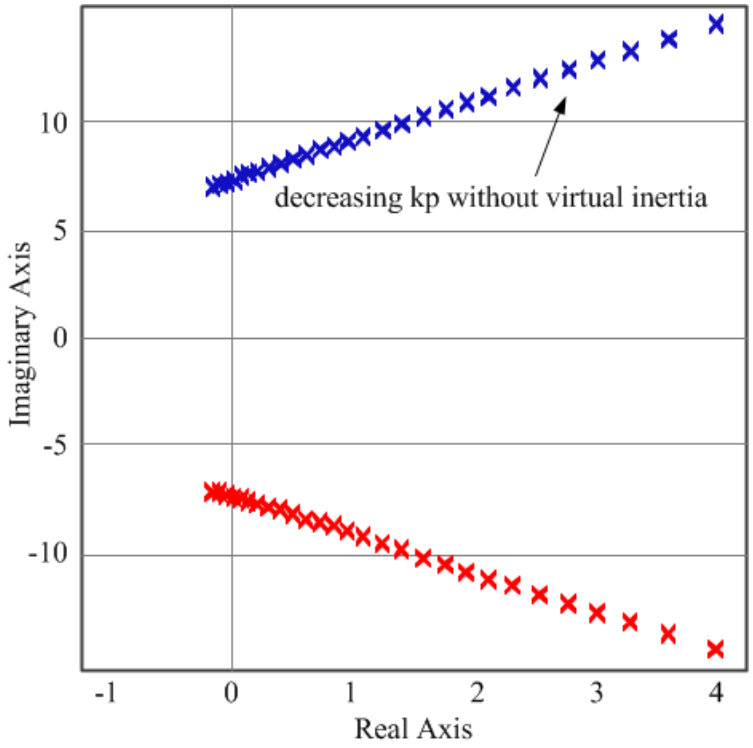


***Fig. 3. Understudy root locus without any virtual inertia affected by $M_v$.***

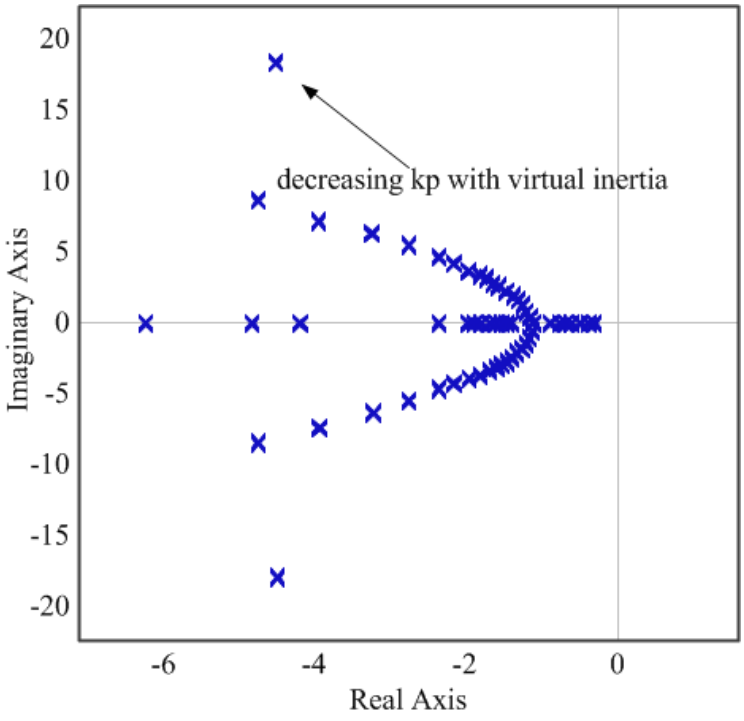


***Fig. 4. Understudy root locus with virtual inertia affected by $K_p$.***

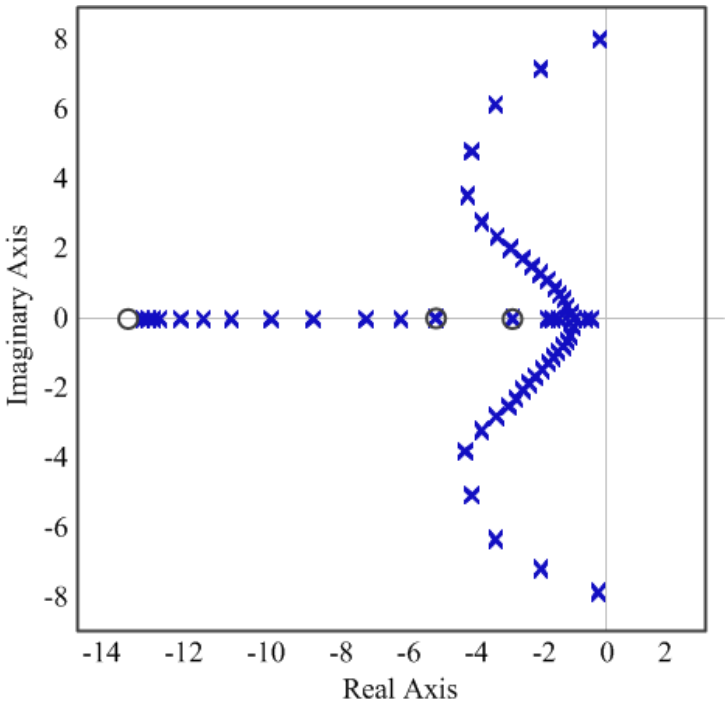


***Fig. 5. Understudy root locus affected by $M_v$.***

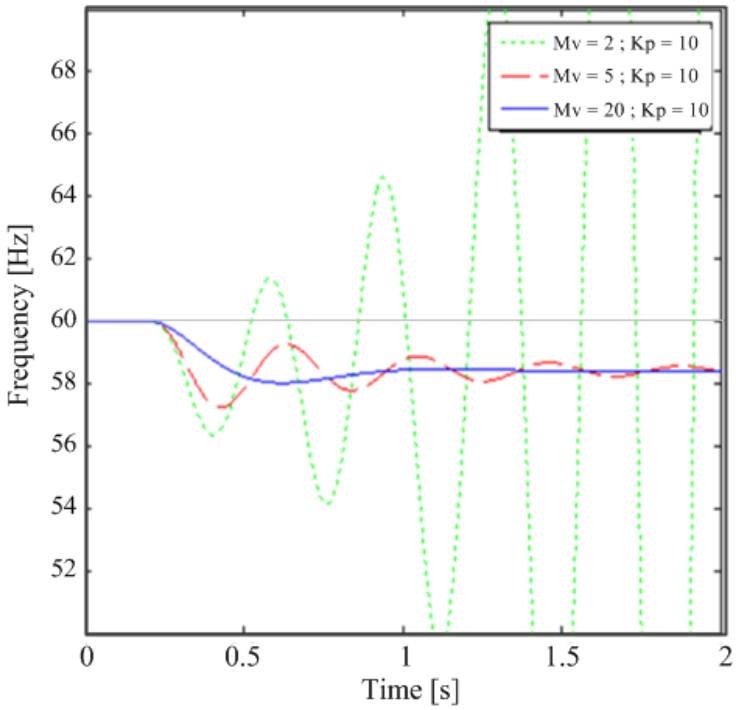


***Fig. 6. Frequency variation as $M_v$ different values and $K_p$ in equation 10.***

Figure 4 denotes that virtual inertia addition leads to improvement of the understudy micro-grid stability so that the system would be steadily equal to 1 even by

$K_p$ low values.

In Figure 5 system root locus considering $M_v$ variation is shown. In this mode $K_p$ value is supposed 114 constant. In order to watch the virtual inertia effect on root locus $M_v$ value varies between 0 and 50 seconds. As seen in figure 5 $M_v$ value increment improves system stability.

In figure 6 and 7, the system frequency variation via $K_p$ and $M_v$ different values and load step-like variation at 0.2 seconds are shown. As shown in Figure 6, $M_v$ increment improves system dynamic stability. This way, $M_v$ increment does not have any effect on frequency loss in steady mode. Figure 7 shows a particular mode that $M_v$ value equals 10 constantly. Thus, it denotes that $K_p$ value reduction reduces frequency loss in steady mode. Although $K_p$ decrement and $M_v$ increment improve dynamic stability and system frequency adjustment, but virtual inertia usage has some limitations. According to equation 10, it is not possible to use virtual inertia at low and high wind speeds due to wind turbine stop.

In this mode, low values of $K_p$ cause system instability. On the other hand, if there is confusion in system frequency at high wind speeds and $M_v$ high values, the generator will produce additional power by virtual inertia control loop operation, and generator temperature increases that may be over-limited. Thus it is not possible to increase $M_v$ till a high value due to these limitations because the system would be going to have frequency loss and weak dynamic stability.

## 4. PROPOSED FREQUENCY CONTROL SYSTEM

In order to adjust the frequency and steady mode fault elimination, in classic load-frequency control systems a control loop consisting of an integrator is added to the control system.

By the way, these classic load-frequency control systems do not operate well up to controlling factors uncertainty. One of them is system input factors uncertainty or factors that exist in the system. In the understudy micro-grid classic load-frequency control system cannot operate well due to $M_v$ and $K_p$ factors uncertainty.

As mentioned in the last part, $K_p$ value decrement causes frequency variation reduction in steady mode although reduces dynamic system stability. It is not also possible to increase $M_v$ to a high value due to thermal limitations. In order to improve dynamic stability, frequency variation reduction in steady mode and also appropriate operation of frequency control system while $K_p$ and $M_v$ different parameters, in this paper a $Robust\ H_\infty$ combined strict controller is suggested.

$Robust\ H_\infty$ combined strict controller is used in reference [21-23] for the load-frequency control loop. This controller is a multi-purpose combined controller that is used to assure closed-loop system operation and stability up to high frequencies that are not dynamically modeled.

Not only $Robust\ H_\infty$ combined strict controller can operate as a strict and flexible control but also optimizes operation at frequency region. Indeed, $H_\infty$ combined strict controller is more suitable than $Robust\ H_\infty$ strict controller because besides the strict stability, it has optimized operation in the load-frequency control loop.

To design this controller first we should obtain system transfer function shown in Figure 2 according to $\Delta\omega$ to $Load\ Ref$ ratio. System transfer function $G_m(s)$ displays $kN(s)$ to $D(s)$ ratio so that $N(s)$ and $D(s)$ indicate system zeros and poles. The main form of this transfer function is shown as follows:

$$G_m(s) = \frac{kN(s)}{D(s)} = k\frac{(s+z_1)(s+z_2)\ldots}{(s+p_1)(s+p_2)\ldots} \quad (13)$$

Where $p_i$ and $z_i$ and $k$ values are in Table 2.

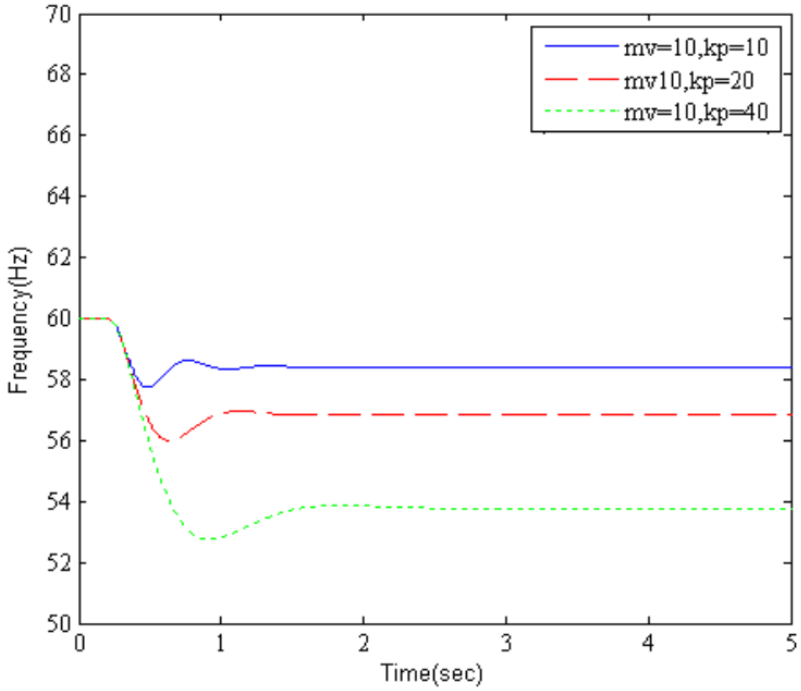


***Fig. 7. Frequency variation as $K_p$ different values and $M_v$.***

**Table 2.** ***Factors value in the transfer function $G_m(s)$.***

| | | | |
|---|---|---|---|
| K | 3821 | P1 | -9.001 |
| Z1 | -9.002 | P2 | -2551 |
| Z2 | -2650 | P3 | -21.61 |
| Z3 | -12.78 | P4 | -4.25 |
| Z4 | -5.026 | P5 | -1.999 |
| Z5 | -2.500 | P6 | -1.765 |
| Z6 | -2.001+j 0.310 | P7 | -0.514+j 10.12 |
| Z7 | -2.001-j 0.310 | P8 | -0.514-j 10.12 |

**Table 3.** ***Factors value in the transfer function*** $G_m(s)$**.**

| $\delta_{kp}$ | $K'_p$ | $\rho_{kp}$ | $\delta_{mv}$ | $m'_v$ | $\rho_{m_v}$ |
|---|---|---|---|---|---|
| -117.02 | 103.54 | 24.03 | -48.36 | 12.12 | 19.88 |

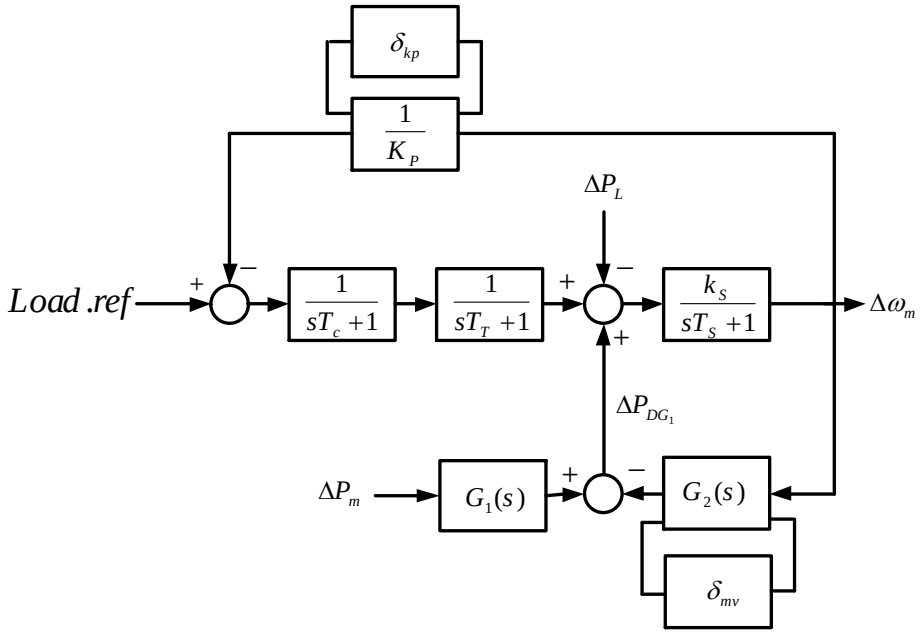


***Fig. 8. Understudy block diagram with uncertainty.***

### 4.1. System Uncertainties Modelling

According to the understudy system block diagram $M_v$ and $K_p$ factors variation effect could be applied in the following relations:

$$\frac{1}{K_p} = \frac{1}{K'_p(1+\rho_{kp}\delta_{kp})} = \frac{1}{K'_p} - \frac{\rho_{kp}}{K'_p}\delta_{kp}(1+\rho_{kp}\delta_{kp})^{-1} = F(M_{kp},\delta_{kp}) \quad (14)$$

We have $0 < \rho_{kp} < 1$ and $F(M_{kp},\delta_{kp})$ is uncertainty matrix appearance via *LFT* form is for uncertainty and as a result:

$$M_{kp} = \begin{bmatrix} -\rho_{kp} & \frac{1}{K'_p} \\ -\rho_{kp} & \frac{1}{K'_p} \end{bmatrix} \quad (15)$$

The same for $M_v$ we have:

$$m_v = F(M_{kp},\delta_{kp})$$
$$M_{m_v} = \begin{bmatrix} 0 & m_v{}' \\ \rho_{m_v} & m_v{}' \end{bmatrix} \quad (16)$$

At above relations $\rho_{m_v}, m'_v, \delta_{mv}, \rho_{kp,}$ $K'_p, \delta_{kp}$ in order are: virtual inertia variation percentage, virtual inertia normal value, virtual inertia variation limitation, droop factor variation percentage, droop factor normal value, and droop factor variation

limitation. These factors' values are given in Table 3.

This way we can replace matrixes of $K_p$ and $M_v$ factors with applied changes (that are shown above) in the understudy system block diagram. Understudy micro-grid block diagram considering $M_v$ and $K_p$ is shown in figure 8.

In order to design a strict controller we can see the simple block diagram shown in Figure 8 as the block diagram shown in Figure 9.

### 4.2. Control Problem Definition

As already mentioned, the purpose of this paper is to strict controller design for system so as assure system stability and operation nevertheless system uncertainties. Also, we want to minimize the control signal energy average. So we suppose $K(s)$ strict controller (shown in Figure 9) as a $Robust\ H_\infty$ controller. This way system uncertainties are shown as l *ft* above and $w_p$, $w_u$ and $w_e$ are weight functions. So control problem is to find a controller that supports these terms:

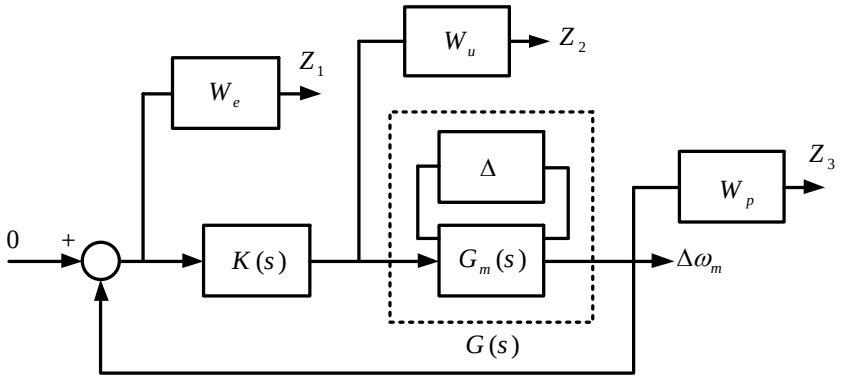


***Fig. 9. Close loop system construction with controller and weight functions.***

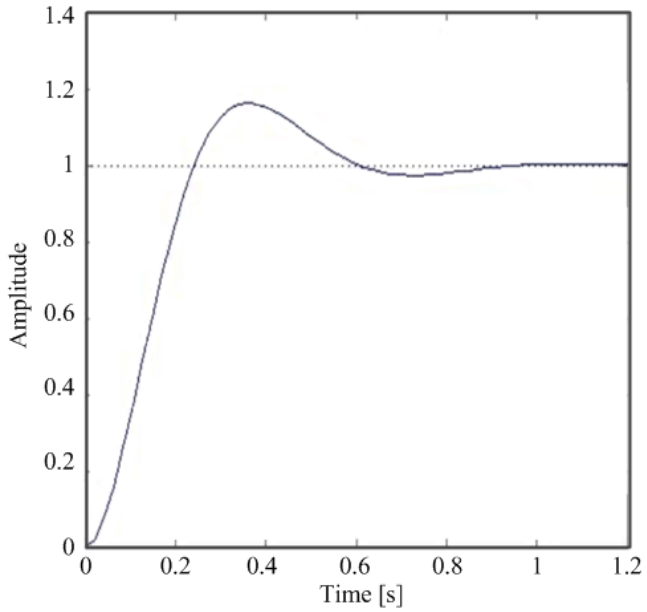


***Fig. 10. Desirable system dynamic step response.***

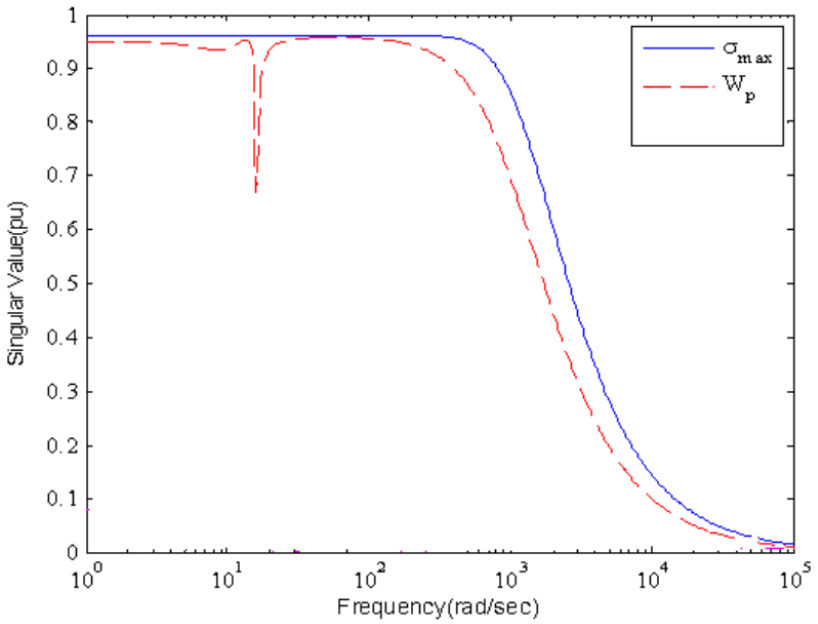


***Fig. 11. Frequency response and close-loop system special value curve.***

$$Y_{opt} = \underset{y}{Min} \left\| \begin{matrix} W_p T \\ W_e S \end{matrix} \right\| < 1 \qquad (17)$$
$$subject\ to: \left\| W_u \right\|_2 < \gamma_2$$

Here $t$ is close loop system transfer function that is as same as the sensitivity supplement function and s is the system sensitivity function.

It means that optimization occurs only for making an optimized compromise between strict stability and efficiency in a normal infinity region. In addition to strict stability, stability optimization and control system efficiency are added to the problem.

### 4.3. Choosing Weight Functions

Weight functions play a principal role in frequency response forming and approach to desirable form. These functions are obtained by identity methods and system primary science.

To compute $W_e$ for desirable response achievement in time region, landing time (ts) should be less than 1s and jumping time (m) should be less than 20 percent. Thus, if a closed loop system has a second-order dominant dynamic, we would have:

$$M = exp\left(\frac{\pi\xi}{\sqrt{1-\xi^2}}\right) < 0.2 \rightarrow \xi > 0.45 \rightarrow \xi = 0.5 \qquad (18)$$

$$T_s = \frac{4}{\xi\omega_n} < 1 \rightarrow \omega_n > 8 \rightarrow \omega_n = 10\frac{rad}{s} \qquad (19)$$

$$T_{id}(s) = \frac{\omega_n^2}{s^2 + 2\omega_n\xi + \omega_n^2} = \frac{100}{s^2 + 10s + 100} \qquad (20)$$

Desirable system step respond $T_{id}(s)$ that is plotted in Figure 10, shows that this ideal transfer function has all desirable expectations.

Now regarding design purpose that is

$||W_e||_\infty < 1$, we can compute $W_e$ transfer function using these relations:

$$S(s) = 1 - T_{id}(s) = 1 - \frac{100}{s^2 + 10s + 100} \quad (21)$$

$$W_e < \frac{1}{S(s)} \quad (22)$$

In order to achieve system stability increment, we move the pole located on the transfer function origin and add a far pole until obtain a pure weight function. So $W_e$ becomes as follows:

$$W_e = \frac{s^2 + 10s + 100}{(s + 0.01)(s + 10)(1 + 0.001s)} \quad (23)$$

According to Figure 9, we can conclude that $W_p$ is as same as $W_e$ weight function. Also regarding equation 19 and the control signal optimized value produced by $K(s)$ controller, it is simple to assume $W_u = 1$.

### 4.4. Combined Controller Design

After the weight functions definition, the controller is designed by a strict control toolbox of MATLAB software. Obtained strict controller special values $K(s)$ are listed in Table 4. As shown in Table 4, the design result is a 10-order controller in order to simplify it, controller order is reduced to 5 orders by strict control toolbox equipment of MATLAB software usage.

Figure 11 displays the closed-loop system maximum value $\delta_{max}$ and weight function frequency response. As it is obvious, terms in equation 18 are verified.

According to Figure 11, the closed loop system maximum value is flat in a wide frequency range and the maximum value is 0.9416.

Figure 12 shows the final understudy system modeling with a designed strict controller.

## 5. SIMULATION RESULTS

Figures 13 and 14 denote $Robust\ H_\infty$ strict

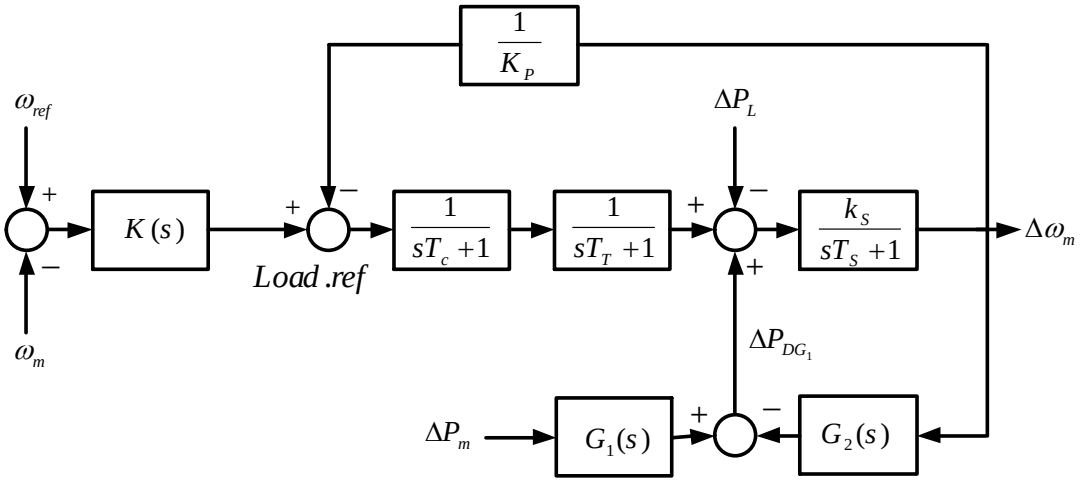


***Fig. 12. System block diagram with controller.***

**Table 4.** ***Factors value in the transfer function $G_m(s)$.***

| Order (n) | 10 | 5 |
|---|---|---|
| λ1 | -2531.14 | -256.32 |
| λ2 | -998.25 | -998.99 |
| λ3 | -1435.62 | -1444.10 |
| λ4 | -59.12 + j 57.31 | -59.13 + j 54.71 |
| λ5 | -59.12 - j 57.31 | -59.13 - j 54.71 |
| λ6 | -11.52 | - |
| λ7 | 0 | - |
| λ8 | -5.01 | - |
| λ9 | -2.00 + j 0.09 | - |
| λ10 | -2.00 - j 0.09 | - |

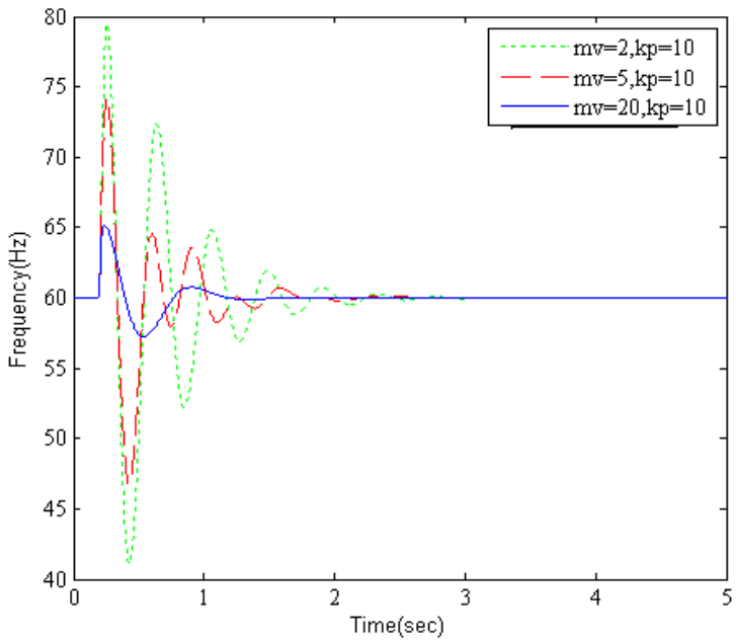


***Fig. 13. Robust $H_\infty$ controller effect on frequency adjustment via $K_p = 10$ and $M_v$ different factors.***

controller addition effect on frequency control system with virtual inertia. In Figure 13, the controller effect on frequencyadjustment via $K_p = 10$ and $M_v$ different values are shown. As it is shown against $M_v$ different values, frequency steady mode fault is always zero. According to Table 4, the reason for steady fault

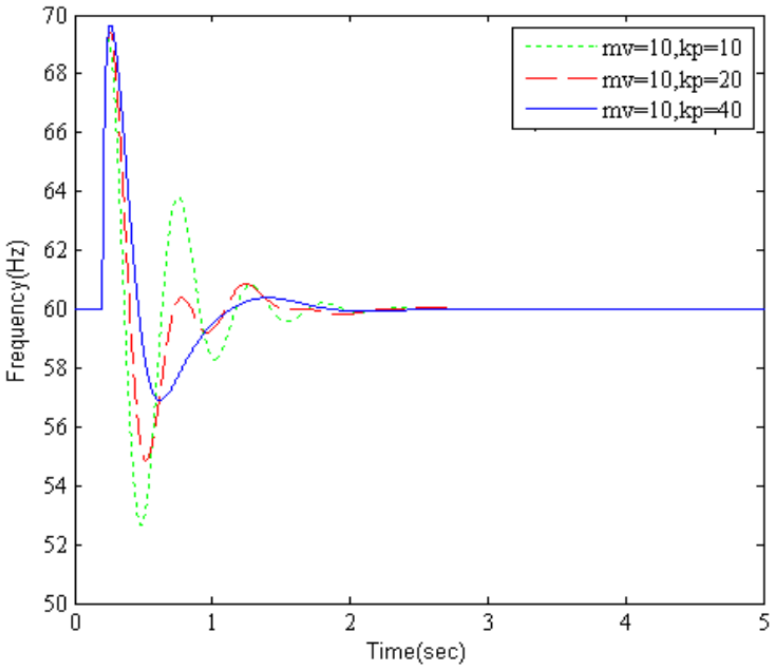


***Fig. 14. Robust $H_\infty$ controller effect on frequency adjustment via $M_v = 10$ and $K_p$ different factors.***

elimination is the existence of a pole in origin $\lambda = 0$ that operates as an integrator. Also, figure 13 shows that $M_v$ value increment improves dynamic system response and reduces maximum frequency variation in transient mode.

Figure 14 shows the strict controller effect on frequency adjustment via $M_v = 10$ and $K_p$ different factors. As it is obvious up to $K_p$ different values, frequency steady mode fault is always zero. Besides, $K_p$ different values do not affect the maximum frequency variation in transient mode. Also according to the curve $K_p$ increment, reduces the transient mode vibrations.

## 6. CONCLUSION

Regarding to stability matter and frequency adjustment in micro-grids, we can improve grid stability using virtual inertia accomplishment. But virtual inertia appropriate operation has some important problems due to uncertainty existence in system model. Thus, in this paper $Robust\ H_\infty$ combined strict controller is suggested and designed so that this controller be strict against droop factor uncertainties at governor system and virtual inertia and also improves system stability.

## REFERENCES

[1] E. Zakieldeen, T. Yi, and L. Yang. "Comparative Study Of Voltage Oriented And Frequency Coordinated Control Of Grid Connected Doubly Fed Induction Generator." journal of renewable and sustainable energy 6.2 (2014): 023120.

[2] J. Jackson John, F. Mwasilu, and J. Jung. "Doubly Fed Induction Generator Wind Turbines: A Novel Integrated

Protection Circuit For Low-Voltage Ride-Through Strategy." journal of renewable and sustainable energy 6.5 (2019): 053129.

[3] M. F. M. Arani, and E. F. El-saadany,"Implementing Virtual Inertia In DFIG-Based Wind Power Generation," ieee transactions on power systems, vol. 28, no. 2, pp. 1373-1384, 2018.

[4] M. Taghizadeh, M. Mohammad, and S. Mokhtar. "A New Method Of Voltage And Frequency Control In Isolated Microgrids Using Enhanced Droop Controller Optimized By Frog Algorithm." journal of renewable and sustainable energy 6.1 (2022): 013136.

[5] R. Ananda-rao, R. Kumuthawathe, A. rosnazri, and s. Taniselass. "Battery Energy Storage System Assessment In A Designed Battery Controller For Load Leveling And Peak Shaving Applications." journal of renewable and sustainable energy 9.4 (2017): 044107.

[6] A. Demiroren,"Automatic Generation Control Using Ann Technique For Multi-Area Power System With Sme Sunits," electric power components and systems, vol. 32, no. 2, pp. 193-213, 2004.

[7] T. Sasaki, T. Kadoya, and K. Enomoto,"Study On Load Frequency Control Using Redox Flow Batteries," ieee transactions on power systems, vol. 19, no. 1, pp. 660-667, 2021.

[8] C. Zhong, and G. Weiss, "Synchronverters: Inverters That Mimic Synchronous Generators," ieee transactions on industrial electronics, vol. 58, no. 4, pp. 1259-1267, 2021.

[9] M. Torres, and L. A. C. Lopes, "Virtual Synchronous Generator Control In Autonomous Wind-Diesel Power Systems," proc. Ieee electrical power & energy conf. (epec), pp. 1-6, 2020.

[10] D. Gautam, L. Goel, R. Ayyanar, V. Vittal, and T. Harbour, "Control Strategy To Mitigate The Impact Of Reduced Inertia Due To Doubly Fed Induction Generators On Large Power Systems," ieee transactions on power systems, vol. 26, pp. 214-224, 2011.

[11] L. R. Chang-chien, E. T. Lin, and E. C. Yin, "Enhancing Frequency Response Control By Dfigs In The High Wind Penetrated Power Systems," ieee transactions on power systems, vol. 26, pp. 710-718, 2018.

[12] M. Nagpal, A. Moshref, G. K. Morison, and p. Kundur, "Experience With Testing And Modeling Of Gas Turbines," ieee power engineering society winter meeting, vol. 2, pp. 652-656, 2001.

[13] Y. Hain, R. Kulesky, and G. Nudelan, "Identificationbased Power Unit Model For Load–Frequency Control Purposes," ieee transactions on power systems, vol. 15, no. 4, pp. 1313- 1321, 2017.

[14] Y. Mi, y. Fu, d. Li, c. Wang, p. C. Loh, and p. Wang, "The Sliding Mode Load Frequency Control For Hybrid Power System Based On Disturbance Observer," electrical power and energy systems, vol. 74, pp. 446-452, 2016.

[15] I. Kocaarslan, c. Ertugrul, "Fuzzy Logic Controller In Interconnected Electrical Power Systems For Load–

Frequency Control," electrical power and energy systems, vol. 27, no. 8, pp. 542-549, 2021.

[16] V. P. Singh, s. R. Mohanty, n. Kishor, and p. K. Ray, "Robust H-Infinity Load Frequency Control In Hybrid Distributed Generation System," electrical power and energy systems, vol. 46, pp. 294-305, 2019.

[17] H. Bevrani, m. R. Feizi, and s. Ataee, "Robust Frequency Control In An Islanded Micro-Grid: H∞/Mu Synthesis Approaches," ieee transactions on smart grid, vol. 7, pp. 706- 717, 2016.

[18] C. Ning, "Robust H∞ Load-Frequency Control In Interconnected Power Systems," iet control theory & applications, vol. 10, pp. 67-75, 2019.

[19] S. A. Saremi hasari, m. Hamzeh, and a. Salemnia, "Dynamic And Static Performance Improvement Of Power Sharing System In Islanded Micro Grids," tjee, vol. 46, no. 1, 2016.

[20] M. Rouholamini, m. Rashidi nejed, and s. Esmaeili, "Simultaneous Scheduling Of Energy And Frequency Control Ancillary Services In Regard To Load Self-Regulation Effect," tjee, vol. 46, no. 1, 2016.

[21] H. Bevrani, and t. Hiyama, "On Load Frequency Regulation With Time Delays: Design And Real-Time Implementation,".ieee transactions on power systems, vol. 24, no. 1, pp. 292-300, 2019.

[22] H. Shayeghi , h. A. Shayanfar, "Design Of Decentralized Robust Lfc In A Competitive Electricity Environment," journal of electrical engineering, vol. 56, no. 9, pp. 225-236, 2015.

[23] H. Shayeghi, "A Robust Decentralized Power System Load Frequency Control," journal of electrical engineering, vol. 59, no. 6, pp. 281-93, 2018.